Electronic Supplementary Information

Impact of Donor Halogenation on Reorganization Energies and Voltage Losses in Bulk-heterojunction Solar Cells

Hongbo Wu[1], Zaifei Ma[1,*], Mengyang Li[1], Hao Lu[2], Ailing Tang[3], Erjun Zhou[3], Jin Wen[1], Yanming Sun[4], Wolfgang Tress[5], Jógvan Magnus Haugaard Olsen[6], Simone Meloni[7,*], Zhishan Bo[2,*], Zheng Tang[1,*]

[1.]State Key Laboratory for Modification of Chemical Fibers and Polymer Materials, Center for Advanced Low-dimension Materials, College of Materials Science and Engineering, Donghua University, 201620 Shanghai, P. R. China
[2.]Key Laboratory of Energy Conversion and Storage Materials, College of Chemistry, Beijing Normal University, 100875, Beijing, P. R. China
[3.]CAS Center for Excellence in Nanoscience National Center for Nanoscience and Technology, 100190 Beijing, P. R. China
[4.]School of Chemistry, Beihang University, 100191 Beijing, P. R. China
[5.]Institute of Computational Physics, Zurich University of Applied Sciences, Wildbachstr. 21, 8401 Winterthur, Switzerland
[6.]DTU Chemistry, Technical University of Denmark, DK-2800 Kongens Lyngby, Denmark
[7.]Dipartimento di Scienze Chimiche, Farmaceutiche e Agrarie – DOCPAS, University of Ferrara, Ferrara, Italy

***Corresponding authors**
mazaifei@dhu.edu.cn (Zaifei Ma)
mlnsmn@unife.it (Simone Meloni)
zsbo@bnu.edu.cn (Zhishan Bo)
ztang@dhu.edu.cn (Zheng Tang)

Keywords: organic solar cell; bulk-heterojunction; donor halogenation; voltage loss; reorganization energy

Table of Contents

Supplementary Note 1. Chemical structures of the active materials

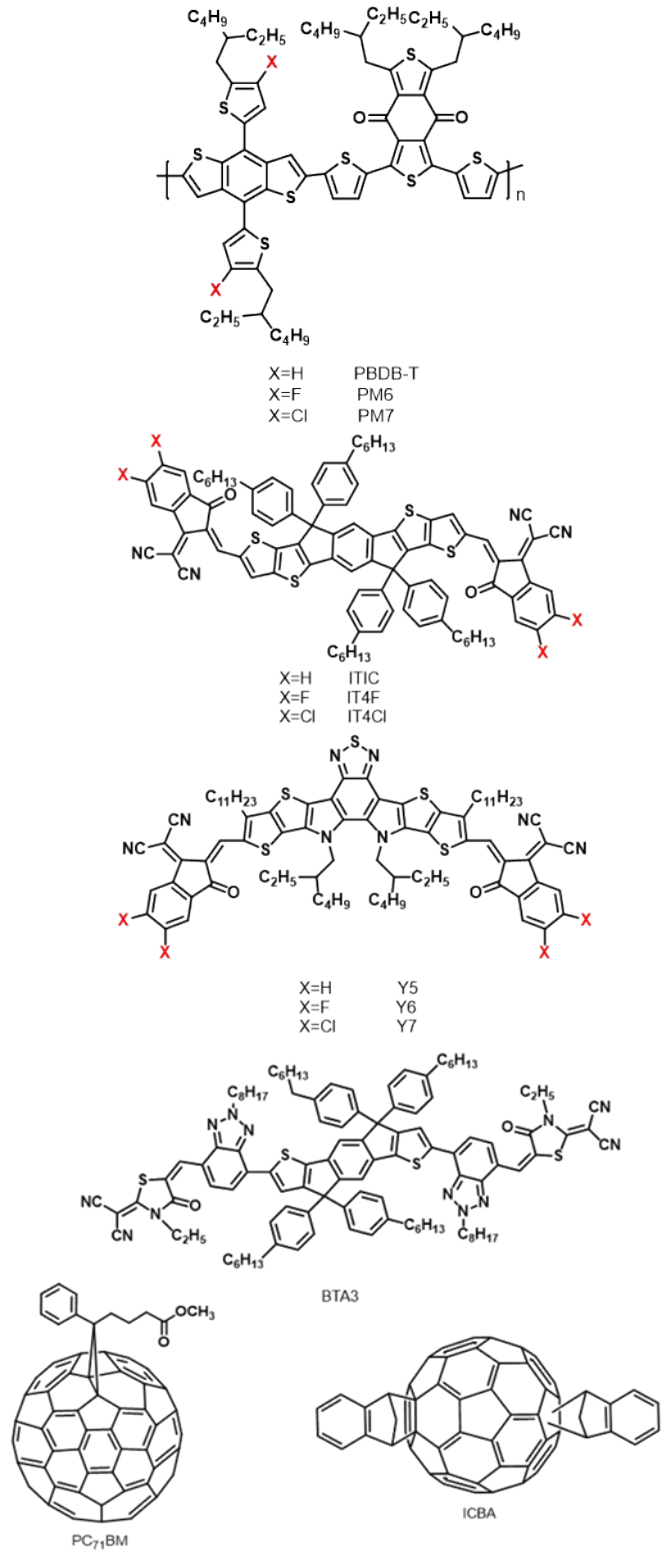

Figure S1. Chemical structures of the active materials used in this work.

Supplementary Note 2. Determination of bandgap energy

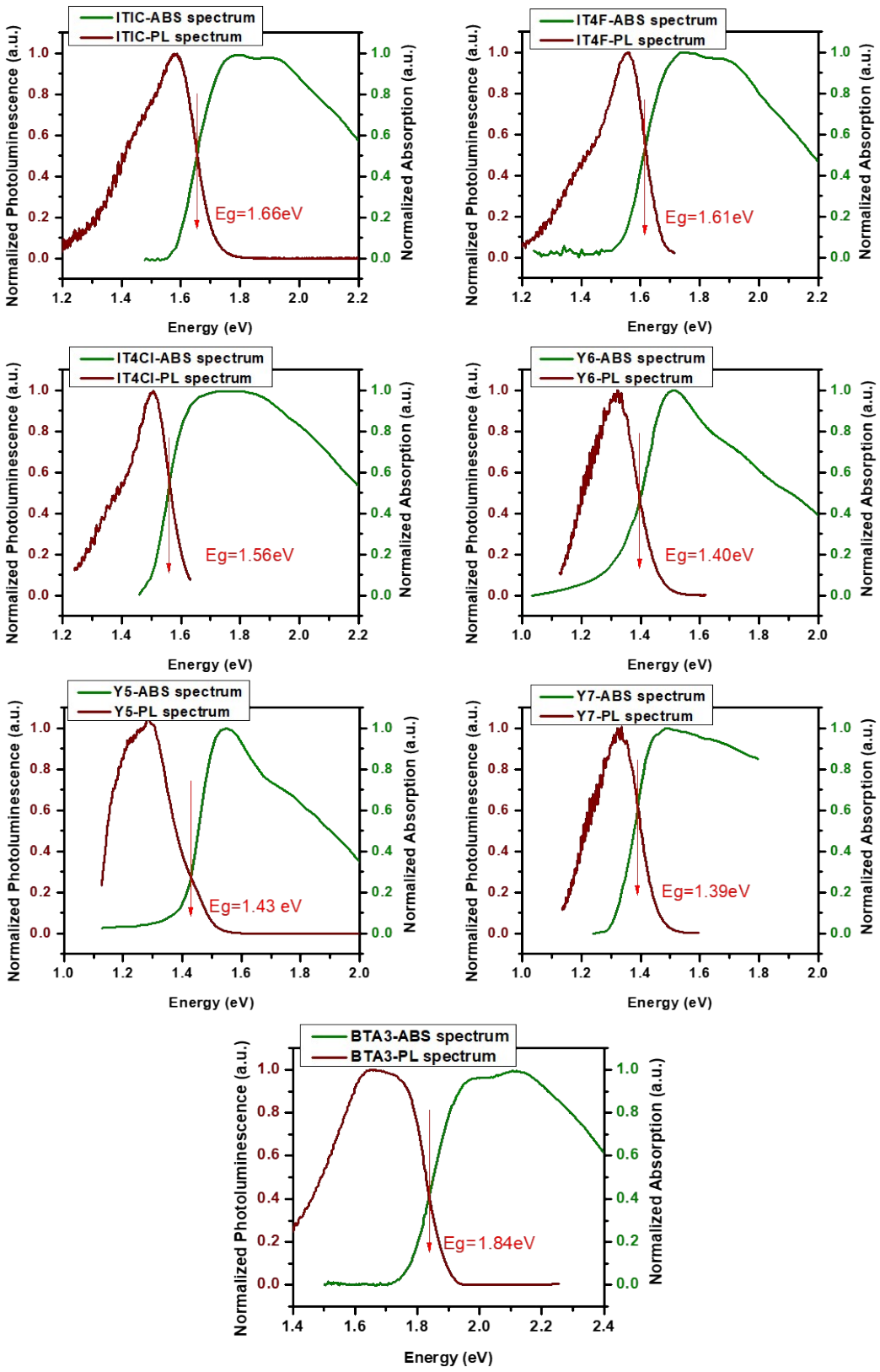

Figure S2. Normalized reduced absorption and photoluminescence spectra of the films of the acceptors. E_g values are taken at the crossing point of the normalized absorption and photoluminescence spectra.

Supplementary Note 3. Photovoltaic performance parameters of the solar cells studied in this work

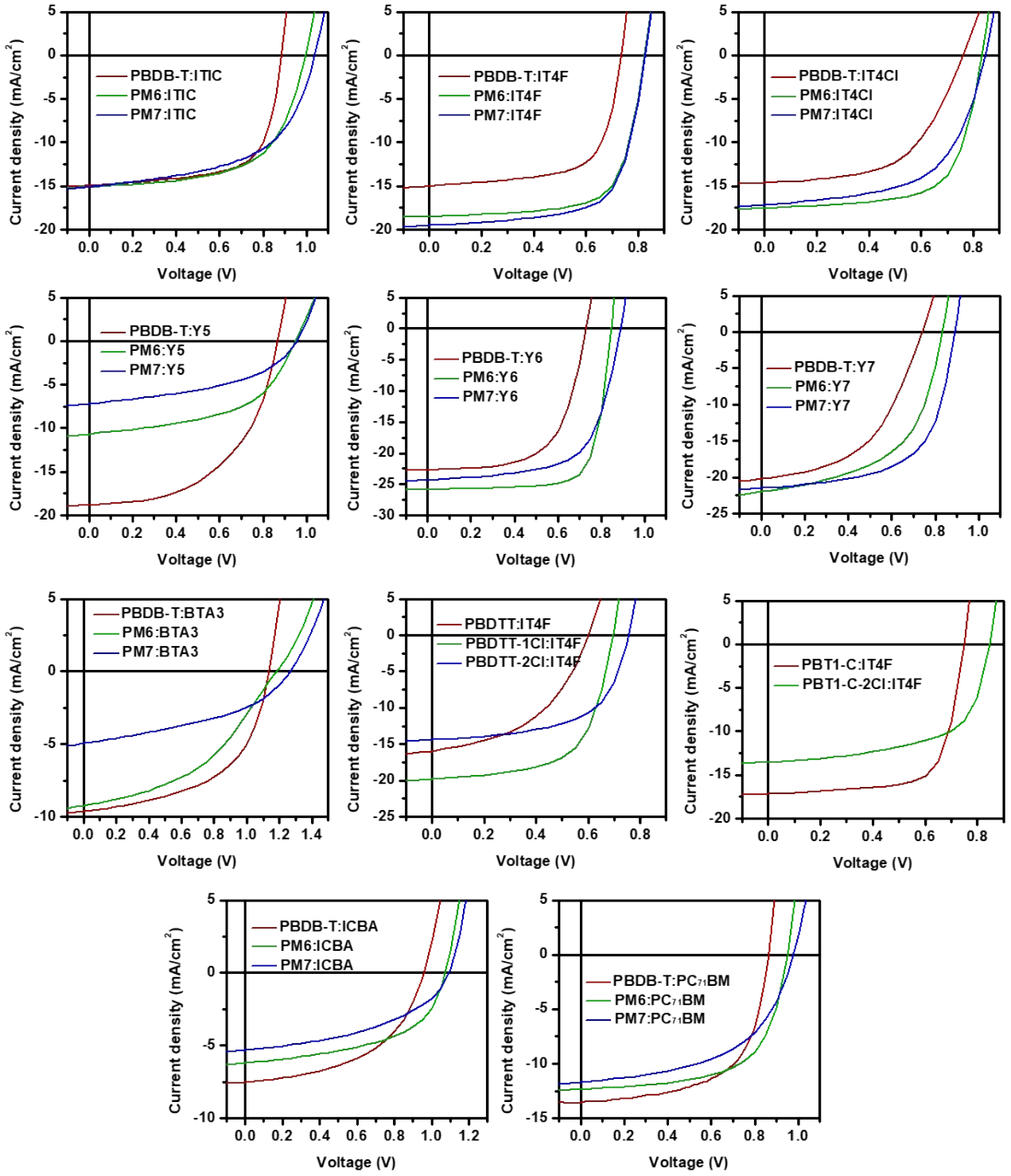

Figure S3. *J-V* curves of the BHJ solar cells based on the polymer donors PBDB-T, PBDTT, PBT1-C, and their halogenated derivatives, mixed with different acceptors.

Table S1. Summary of photovoltaic performance parameters of the BHJ solar cells based on the polymer donors PBDB-T, PBDTT, PBT1-C, and their halogenated derivatives, mixed with different acceptors.

Active Materials	Voc (V)	Jsc (mA/cm^2)	FF (%)	PCE (%)
PBDB-T:ITIC	0.89(0.88±0.005)	14.93	66.8	8.80
PM6:ITIC	1.00(1.00±0.005)	15.10	60.4	9.07
PM7:ITIC	1.04(1.04±0.005)	15.09	54.8	8.64
PBDB-T:IT4F	0.73(0.72±0.010)	14.97	66.8	7.33
PM6:IT4F	0.82(0.82±0.010)	18.47	69.7	10.61
PM7:IT4F	0.83(0.83±0.010)	19.52	67.5	10.90
PBDB-T:IT4Cl	0.76(0.76±0.005)	14.63	55.7	6.18
PM6:IT4Cl	0.83(0.83±0.005)	18.52	67.1	10.31
PM7:IT4Cl	0.85(0.85±0.005)	17.10	58.3	8.44
PBDB-T:BTA3	1.14(1.14±0.010)	9.62	53.4	5.83
PM6:BTA3	1.18(1.18±0.010)	9.23	42.8	4.67
PM7:BTA3	1.27(1.27±0.010)	4.94	41.5	2.59
PBT1-C:IT4F	0.75(0.75±0.005)	17.15	70.5	9.07
PBT1-C-2Cl:IT4F	0.85(0.85±0.005)	13.50	60.7	6.97
PBDTT:IT4F	0.60(0.60±0.005)	15.92	46.8	4.48
PBDTT-1Cl:IT4F	0.70(0.70±0.005)	19.77	62.0	8.51
PBDTT-2Cl:IT4F	0.76(0.76±0.005)	14.40	58.8	6.44
PBDB-T:Y5	0.87(0.87±0.005)	18.82	52.4	8.56
PM6:Y5	0.95(0.95±0.005)	10.66	52.2	5.28
PM7:Y5	0.96(0.96±0.005)	7.17	45.8	3.13
PBDB-T:Y6	0.73(0.73±0.005)	22.69	62.3	10.32
PM6:Y6	0.84(0.84±0.005)	25.81	75.2	16.41
PM7:Y6	0.89(0.89±0.005)	24.30	64.6	13.97
PBDB-T:Y7	0.74(0.74±0.005)	20.22	49.6	7.41
PM6:Y7	0.83(0.83±0.005)	22.00	54.3	9.92
PM7:Y7	0.89(0.89±0.005)	21.50	61.2	11.71
PBDB-T:PC$_{71}$BM	0.86(0.86±0.010)	13.55	60.5	7.05
PM6:PC$_{71}$BM	0.95(0.95±0.010)	12.35	62.2	7.30
PM7:PC$_{71}$BM	0.98(0.98±0.010)	11.69	53.0	6.04
PBDB-T:ICBA	0.95(0.95±0.010)	7.50	50.3	3.58
PM6:ICBA	1.07(1.07±0.010)	6.20	52.5	3.48
PM7:ICBA	1.09(1.09±0.010)	5.32	44.9	2.61

Supplementary Note 4. Details regarding the determination of $V_{oc,rad}$

For a solar cell, $V_{oc,rad}$ is defined as the open-circuit voltage for the device without non-radiative recombination loss (ΔV_{nr}), or in other words, with 100% EQE_{EL}, which means that every electron injected into the device is converted to a photon[1]. According to the detailed balance theory[2], $V_{oc,rad}$ is determined by J_{sc} and $J_{0,rad}$, via

$$V_{oc,rad} = \frac{kT}{q}\ln\left(\frac{J_{sc}}{J_{0,rad}} + 1\right) \quad \text{(eq. S4.1)}$$

where k is the Boltzmann constant, T is temperature, q is elementary charge, and $J_{0,rad}$ is the radiative limit for the dark saturation current of the device. $J_{0,rad}$ can be expressed as

$$J_{0,rad} = q\int EQE_{PV}(E)BB(E)dE \quad \text{(eq. S4.2)}$$

where $EQE_{PV}(E)$ is the photovoltaic external quantum efficiency of the solar cell, $BB(E)$ is the blackbody emission photon flux at room temperature (300 K). Because blackbody photon flux exponentially reduces with increasing photon energy[3] in the energy range of interest, the lower energy part of the EQE_{PV} spectrum is critically important in determining $J_{0,rad}$. Thus, the determination of $J_{0,rad}$, using equation S4.2., requires an accurate measurement of the tail of the EQE_{PV} spectrum. For this purpose, we measure the electroluminescence spectra (*EL(E)*) of the organic solar cells studied in this work, using a highly sensitive setup. Then, we calculate the spectral shape of the tail of EQE_{PV}, using the reciprocal relation[4], following

$$EL(E) = EQE_{PV}(E)BB(E)\left[\exp\left(\frac{qV}{kT}\right) - 1\right] \quad \text{(eq. S4.3)}$$

where V is the voltage over the solar cell. The calculated spectral shape of the EQE_{PV} tail is attached to the measured sensitive EQE_{PV} spectrum of the device, extending the range of EQE_{PV} to 10 orders of magnitude. As a result, $J_{0,rad}$ and thus $V_{oc,rad}$ can be determined. Below are the sensitive EQE_{PV} spectra of the solar cells studied in this work. The calculated $J_{0,rad}$ and $V_{oc,rad}$ values are listed in **Table S2**.

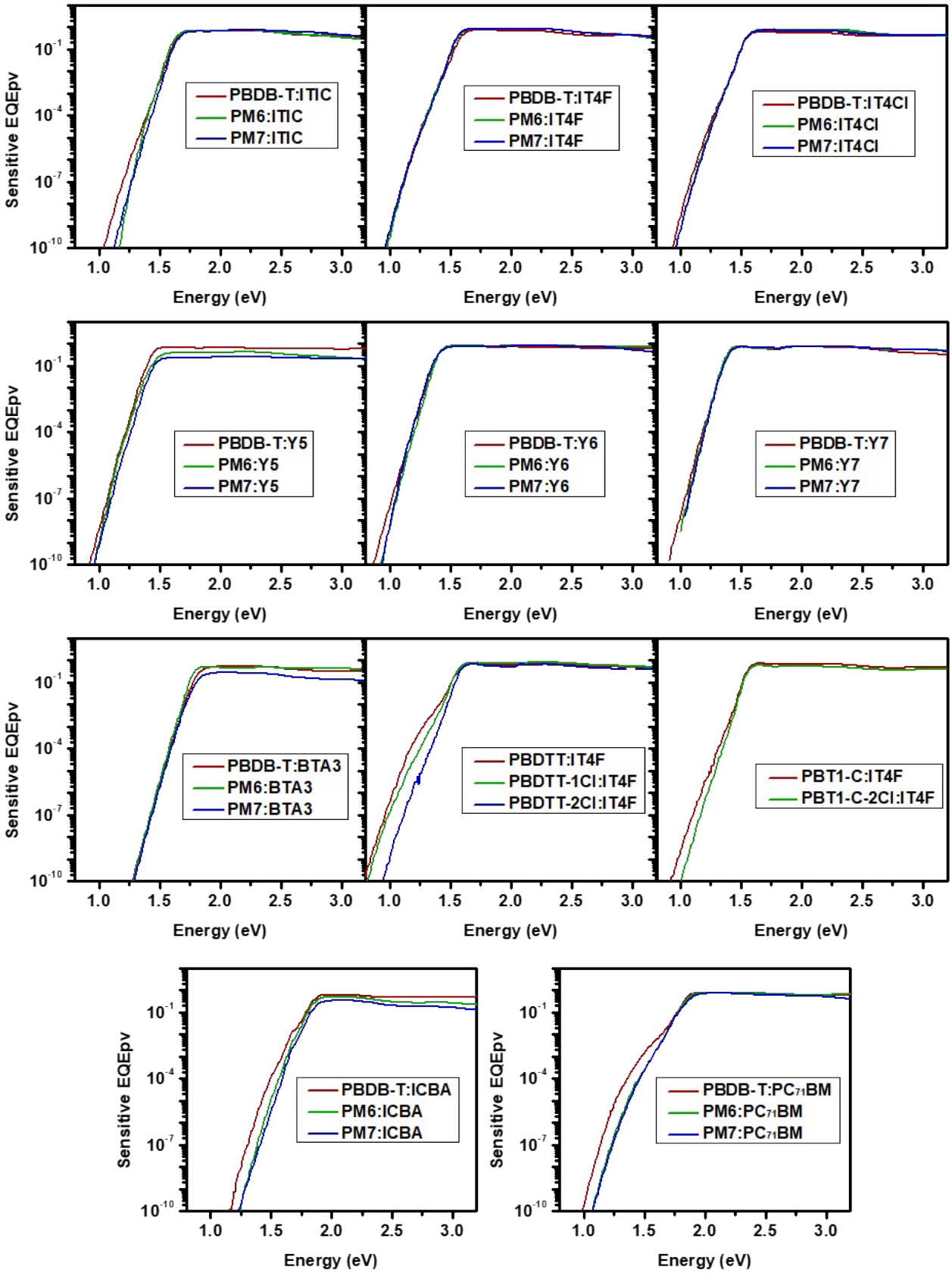

Figure S4. Sensitive EQE_{PV} spectra for the solar cells based on based on the polymer donors PBDB-T, PBDTT, PBT1-C, and their halogenated derivatives, mixed with different acceptors.

Table S2. Summary of the saturation current $J_{0,rad}$, J_{SC} calculated from EQE_{PV}, and $V_{oc,rad}$ of the organic solar cells based on the polymer donors PBDB-T, PBDTT, PBT1-C, and their halogenated derivatives, mixed with different acceptors.

Active Materials	$calc.J_{sc}$ (mA/cm²)	$J_{0,rad}$ (A/m²)	$V_{oc,rad}$ (V)
PBDB-T:ITIC	15.19	$7.6x10^{-20}$	1.226
PM6:ITIC	14.59	$3.0x10^{-20}$	1.248
PM7:ITIC	14.67	$1.3x10^{-20}$	1.269
PBDB-T:IT4F	15.41	$1.7x10^{-18}$	1.149
PM6:IT4F	18.95	$1.5x10^{-18}$	1.158
PM7:IT4F	18.97	$1.5x10^{-18}$	1.157
PBDB-T:IT4Cl	13.58	$4.8x10^{-18}$	1.120
PM6:IT4Cl	18.10	$2.4x10^{-18}$	1.144
PM7:IT4Cl	16.49	$2.1x10^{-18}$	1.146
PBDB-T:BTA3	8.63	$3.7x10^{-23}$	1.403
PM6:BTA3	8.88	$6.1x10^{-23}$	1.391
PM7:BTA3	4.27	$2.4x10^{-23}$	1.396
PBT1-C:IT4F	16.31	$2.7x10^{-18}$	1.139
PBT1-C-2Cl:IT4F	12.83	$3.9x10^{-19}$	1.181
PBDTT:IT4F	15.91	$5.2x10^{-17}$	1.064
PBDTT-1Cl:IT4F	18.91	$9.6x10^{-18}$	1.111
PBDTT-2Cl:IT4F	14.24	$1.4x10^{-18}$	1.153
PBDB-T:Y5	19.09	$3.8x10^{-17}$	1.077
PM6:Y5	10.62	$1.8x10^{-17}$	1.081
PM7:Y5	6.79	$6.5x10^{-18}$	1.095
PBDB-T:Y6	21.72	$1.8x10^{-16}$	1.041
PM6:Y6	24.57	$7.6x10^{-17}$	1.066
PM7:Y6	23.28	$1.6x10^{-16}$	1.046
PBDB-T:Y7	19.87	$1.4x10^{-16}$	1.045
PM6:Y7	21.60	$1.3x10^{-16}$	1.049
PM7:Y7	21.14	$9.3x10^{-17}$	1.057
PBDB-T:$PC_{71}BM$	13.22	$5.0x10^{-19}$	1.176
PM6:$PC_{71}BM$	12.66	$1.8x10^{-20}$	1.257
PM7:$PC_{71}BM$	11.06	$1.3x10^{-20}$	1.262
PBDB-T:ICBA	6.97	$1.3x10^{-21}$	1.308
PM6:ICBA	6.12	$8.7x10^{-23}$	1.372
PM7:ICBA	4.65	$4.0x10^{-23}$	1.385

Supplementary Note 5. Summary of the voltage loss values

Table S3. Summary of the voltage loss values for the BHJ organic solar cells based on the polymer donors PBDB-T, PBDTT, PBT1-C, and their halogenated derivatives, mixed with different acceptors.

Active Materials	EQE_{EL}	ΔV_{nr} (V)	ΔV_{nr}^{cal} (V)	ΔV_r (V)	ΔV_{loss} (V)	Voc (V)	E_g (eV)
PBDB-T:ITIC	3.1x10^{-6}	0.32	0.34	0.43	0.77	0.89	1.66
PM6:ITIC	8.8x10^{-6}	0.29	0.25	0.41	0.66	1.00	1.66
PM7:ITIC	4.5x10^{-5}	0.25	0.23	0.39	0.62	1.04	1.66
PBDB-T:IT4F	4.0x10^{-7}	0.37	0.42	0.46	0.88	0.73	1.61
PM6:IT4F	5.5x10^{-6}	0.30	0.34	0.45	0.79	0.82	1.61
PM7:IT4F	2.8x10^{-6}	0.32	0.33	0.45	0.78	0.83	1.61
PBDB-T:IT4Cl	1.6x10^{-6}	0.33	0.36	0.44	0.80	0.76	1.56
PM6:IT4Cl	3.3x10^{-6}	0.32	0.31	0.42	0.73	0.83	1.56
PM7:IT4Cl	4.9x10^{-6}	0.31	0.30	0.41	0.71	0.85	1.56
PBDB-T:BTA3	7.2x10^{-5}	0.24	0.26	0.44	0.70	1.14	1.84
PM6:BTA3	5.5x10^{-4}	0.19	0.21	0.45	0.66	1.18	1.84
PM7:BTA3	1.0x10^{-3}	0.17	0.13	00.44	0.57	1.27	1.84
PBT1-C:IT4F	1.8x10^{-7}	0.39	0.39	0.47	0.86	0.75	1.61
PBT1-C-2Cl:IT4F	9.0x10^{-7}	0.35	0.33	0.43	0.76	0.85	1.61
PBDTT:IT4F	5.7x10^{-9}	0.48	0.46	0.55	1.01	0.60	1.61
PBDTT-1Cl:IT4F	2.5x10^{-8}	0.44	0.42	0.49	0.91	0.70	1.61
PBDTT-2Cl:IT4F	4.7x10^{-8}	0.42	0.40	0.45	0.85	0.76	1.61
PBDB-T:Y5	2.0x10^{-4}	0.21	0.21	0.35	0.56	0.87	1.43
PM6:Y5	2.7x10^{-3}	0.15	0.13	0.35	0.48	0.95	1.43
PM7:Y5	4.7x10^{-3}	0.13	0.14	0.33	0.47	0.96	1.43
PBDB-T:Y6	1.3x10^{-6}	0.34	0.32	0.35	0.67	0.73	1.40
PM6:Y6	1.0x10^{-4}	0.23	0.22	0.34	0.56	0.84	1.40
PM7:Y6	4.2x10^{-4}	0.19	0.16	0.35	0.51	0.89	1.40
PBDB-T:Y7	1.6x10^{-6}	0.33	0.31	0.34	0.65	0.74	1.39
PM6:Y7	1.7x10^{-4}	0.22	0.22	0.34	0.56	0.83	1.39
PM7:Y7	5.4x10^{-4}	0.19	0.17	0.33	0.50	0.89	1.39
PBDB-T:$PC_{71}BM$	1.4x10^{-6}	0.34	0.32	0.53	0.85	0.86	1.71[5]
PM6:$PC_{71}BM$	2.0x10^{-6}	0.33	0.31	0.45	0.76	0.95	1.71
PM7:$PC_{71}BM$	6.0x10^{-6}	0.30	0.30	0.43	0.73	0.98	1.71
PBDB-T:ICBA	8.6x10^{-7}	0.35	0.35	0.40	0.75	0.95	1.70[6]
PM6:ICBA	4.6x10^{-6}	0.31	0.31	0.32	0.63	1.07	1.70
PM7:ICBA	2.5x10^{-5}	0.27	0.24	0.37	0.61	1.09	1.70

Supplementary Note 6. Details regarding TPV measurements

Transient photovoltage decay (TPV) measurements are employed to evaluate the impact of donor halogenation on the lifetime of photogenerated charge carriers in organic solar cells. The measurements are done using a LED lamp, driven by a Keithley 2450, for a continues bias illumination, and an additional LED lamp, driven by an arbitrary function generator, for a pulsed illumination. V_{OC} of the solar cells measured under the illumination of the LED lamp operating at maximum current are similar to that measured with a solar simulator. To compare the photovoltage decay lifetime of different solar cells, intensity of the bias illumination is varied for every device. This gives rise to different bias photovoltages (V_{ph}). For each bias illumination intensity, the pulsed illumination is adjusted to increase the photovoltage, temporarily, by about 5%. The decay time of the transient photovoltage generated by the pulsed illumination is recorded by an oscilloscope, and the decay spectrum is fitted by a single exponential decay function for the determination of the decay lifetime. Finally, the decay lifetime values are plotted as a function of V_{ph}. Below, the lifetime vs V_{ph} plots, as well as the transient photovoltage vs time plots, for the different solar cells based on the non-halogenated and the halogenated donors, mixed with different acceptors, are provided.

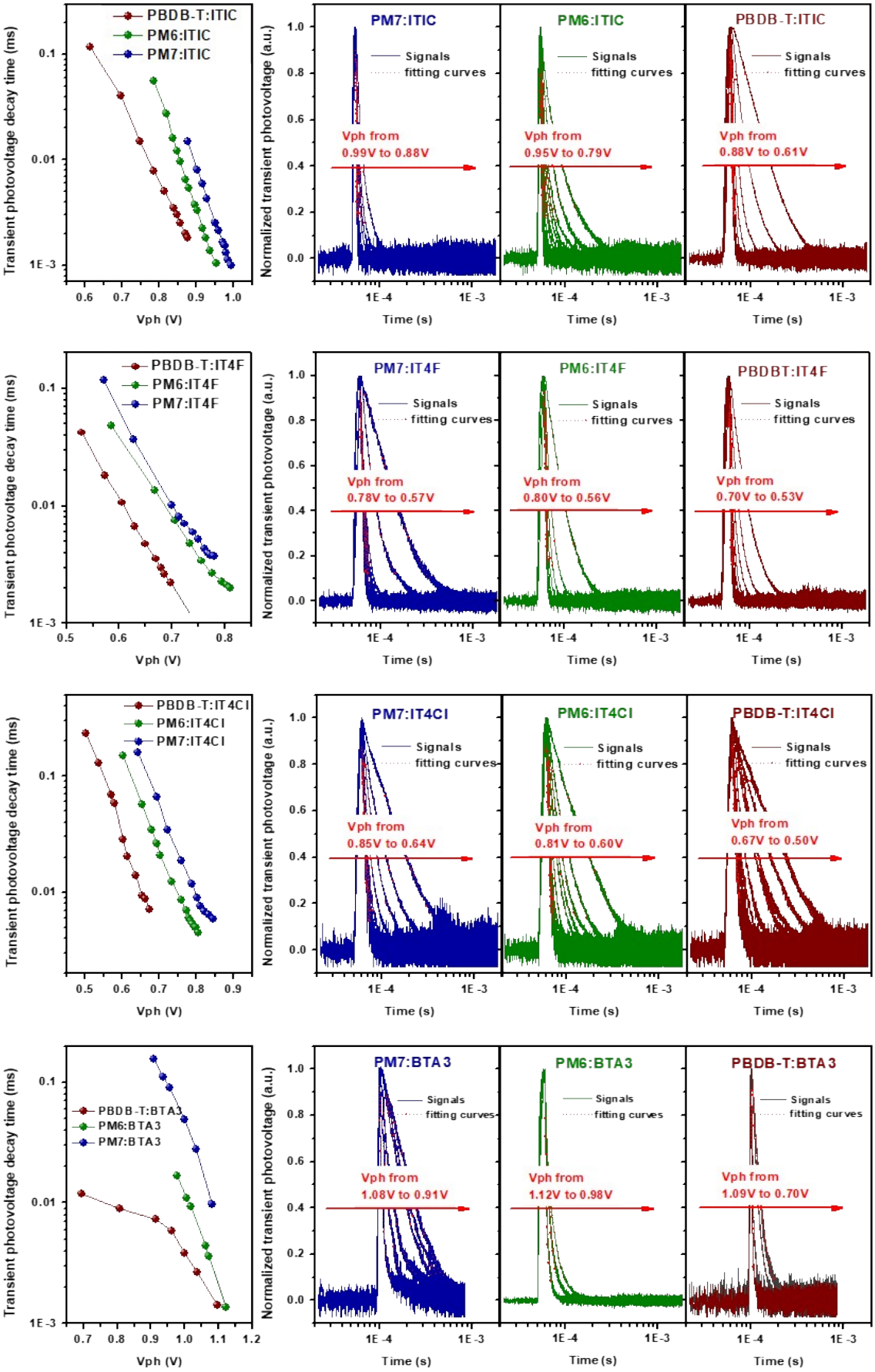
PBDB-T:ITIC
PM6:ITIC
PM7:ITIC
Transient photovoltage decay time (ms)
Vph (V)
Normalized transient photovoltage (a.u.)
Time (s)
Signals
fitting curves
Vph from
0.99V to 0.88V
Vph from
0.95V to 0.79V
Vph from
0.88V to 0.61V
PBDB-T:IT4F
PM6:IT4F
PM7:IT4F
Vph from
0.78V to 0.57V
Vph from
0.80V to 0.56V
Vph from
0.70V to 0.53V
PBDB-T:IT4Cl
PM6:IT4Cl
PM7:IT4Cl
Vph from
0.85V to 0.64V
Vph from
0.81V to 0.60V
Vph from
0.67V to 0.50V
PBDB-T:BTA3
PM6:BTA3
PM7:BTA3
Vph from
1.08V to 0.91V
Vph from
1.12V to 0.98V
Vph from
1.09V to 0.70V

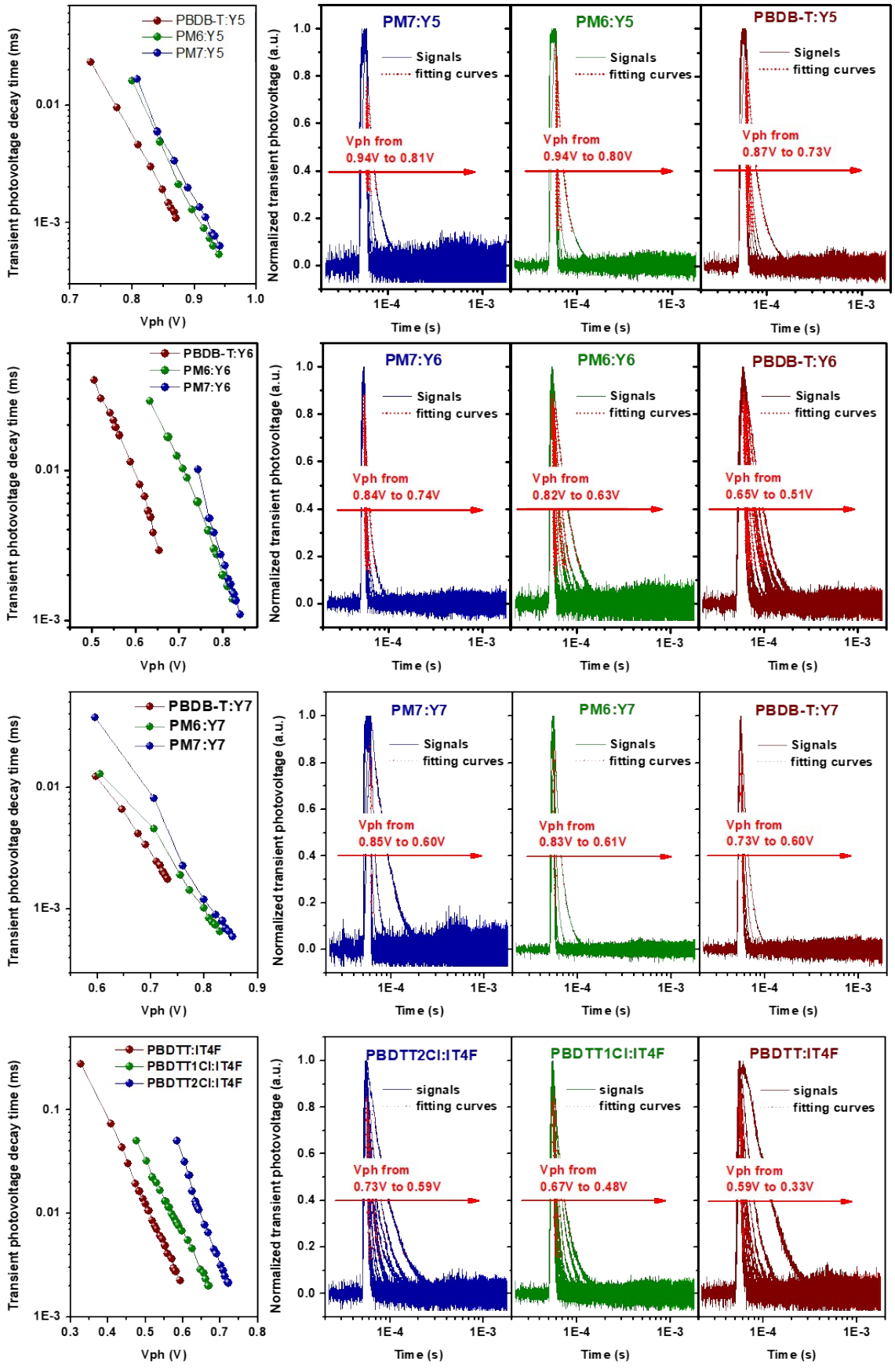
PBDB-T:Y5
PM6:Y5
PM7:Y5
Transient photovoltage decay time (ms)
Vph (V)
Normalized transient photovoltage (a.u.)
Time (s)
PM7:Y5
Signals
fitting curves
Vph from
0.94V to 0.81V
PM6:Y5
Signals
fitting curves
Vph from
0.94V to 0.80V
PBDB-T:Y5
Signels
fitting curves
Vph from
0.87V to 0.73V
PBDB-T:Y6
PM6:Y6
PM7:Y6
PM7:Y6
Signals
fitting curves
Vph from
0.84V to 0.74V
PM6:Y6
Signals
fitting curves
Vph from
0.82V to 0.63V
PBDB-T:Y6
Signals
fitting curves
Vph from
0.65V to 0.51V
PBDB-T:Y7
PM6:Y7
PM7:Y7
PM7:Y7
Signals
fitting curves
Vph from
0.85V to 0.60V
PM6:Y7
Signals
fitting curves
Vph from
0.83V to 0.61V
PBDB-T:Y7
Signals
fitting curves
Vph from
0.73V to 0.60V
PBDTT:IT4F
PBDTT1Cl:IT4F
PBDTT2Cl:IT4F
PBDTT2Cl:IT4F
signals
fitting curves
Vph from
0.73V to 0.59V
PBDTT1Cl:IT4F
signals
fitting curves
Vph from
0.67V to 0.48V
PBDTT:IT4F
signals
fitting curves
Vph from
0.59V to 0.33V

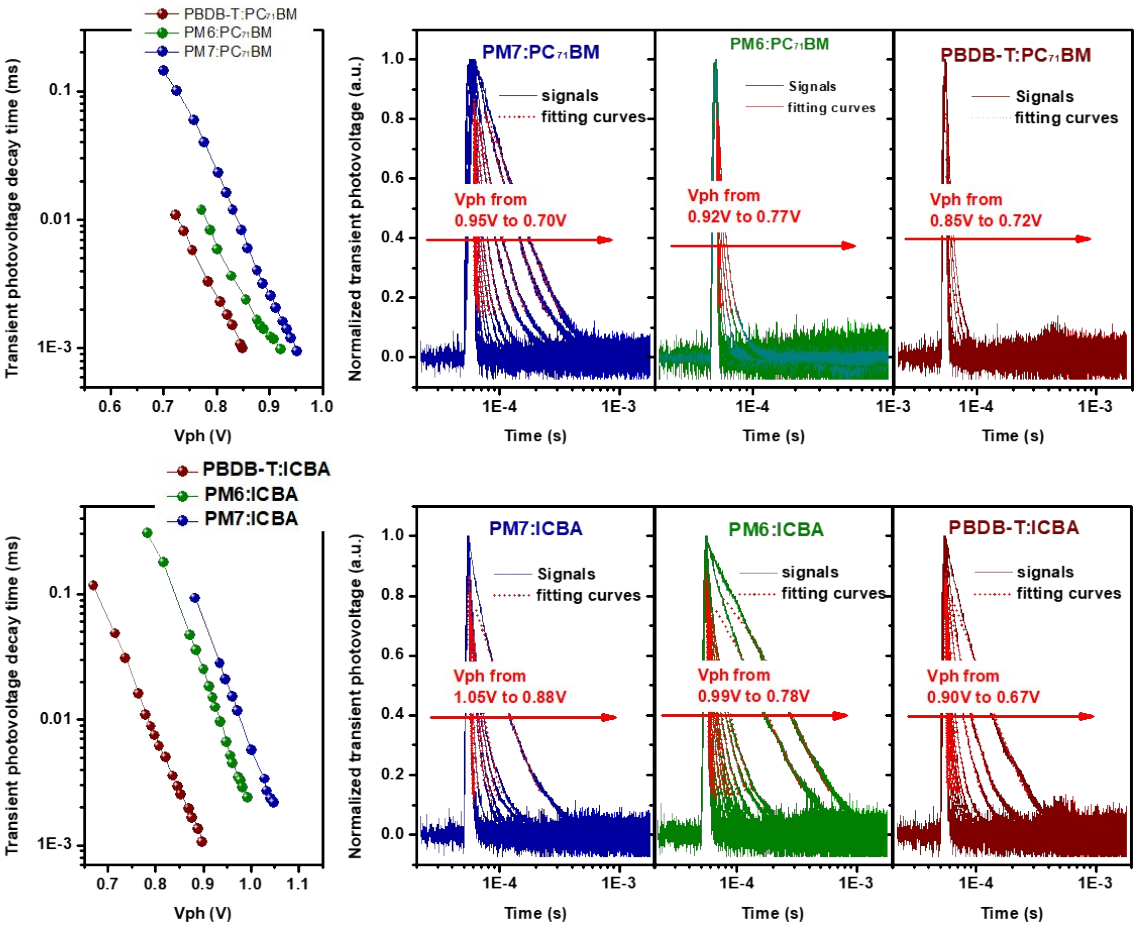

Figure S5. Transient photovoltage decay time as a function of V_{ph} (left), and transient photovoltage decay signals (right) for the solar cells based on non-halogenated and halogenated donors mixed with different acceptors.

Supplementary Note 7. EL spectra and CT state properties of the semitransparent devices

Supplementary Note 7.1. Electroluminescence spectra of the semitransparent devices

In the frame work of Marcus theory[7], the CT state properties of an organic solar cell can be determined by a fitting to the tail of the EQE_{PV} spectrum of the device[7]. This requires an accurate measurement of the tail of the EQE_{PV} spectrum, as discussed in the main text of the manuscript. To extend the range of EQE_{PV}, the electroluminescence (EL) spectrum of the solar cell is measured, and converted to EQE_{PV} spectrum using the reciprocity relation[4]. To avoid optical interference, the solar cell is made semitransparent, using the ITO/ZnO cathode and the MoO_3 (10 nm)/Ag (3 nm) anode. The measured EL spectra of the solar cells studied in this work are provided below.

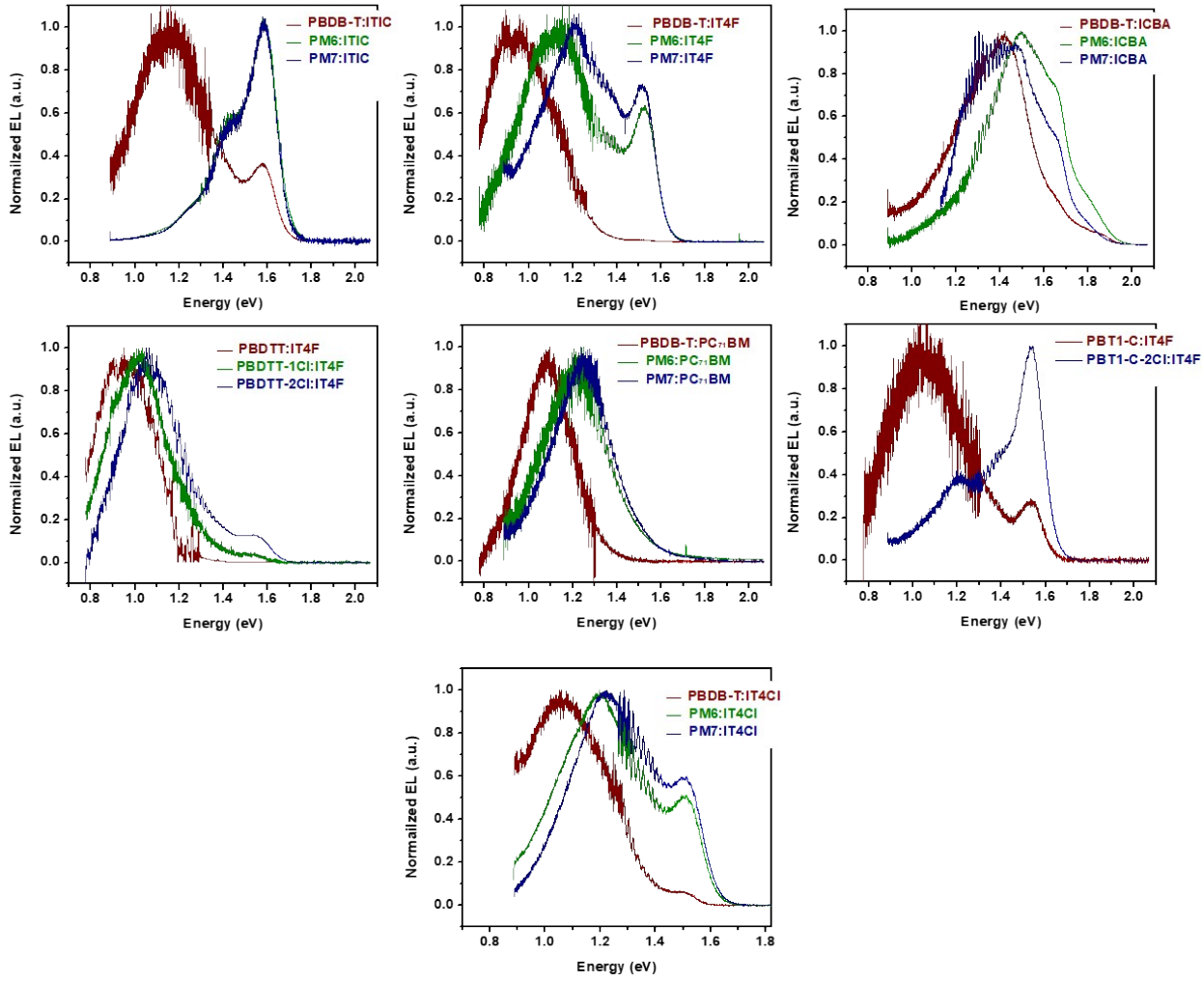

Figure S6. Normalized EL spectra of the semitransparent solar cells based on different active materials systems.

Supplementary Note 7.2. Determination of CT state properties

The CT state properties, namely, the energy of charge transfer state (E_{CT}), the reorganization energy (λ_{CT}) and the oscillator strength (f_{osc}), et al., determine the degree of voltage loss in organic solar cells. To determine the CT state properties, EQE_{PV} spectra of the solar cells constructed in this work are measured using a sensitive EQE_{PV} setup, and the tails of the EQE_{PV} spectra are further extended using the spectra calculated from EL (using the reciprocal relation), following the method reported in the literature[8].

Then, we use equation eq. S7.1 to fit the tails of the EQE spectra,

$$EQE_{PV}(E) = \frac{fE}{\sqrt{4\pi\lambda kT}} exp\left(\frac{-\left(E_{CT}+\lambda-E\right)^2}{4\lambda kT}\right) \quad \text{(eq. S7.1)}$$

where E is photon energy and k is the Boltzmann constant, T is temperature. Accordingly, we determine E_{CT}, λ_{CT} and the prefactor f of the solar cells. Note that f is proportional to the product of f_{osc} *and the density of CT states* (N_{CTC}).

To avoid arbitrary fittings, the radiative limited for the recombination voltage loss, derived using the Shockley-Queissor theory, is used as the lower limit for the fit parameters. Also, the peak value of the CT state EQE_{PV} (the fit curve) is set to be lower than 10% of the peak EQE_{PV} contributed by the donor or the acceptor absorption for the determination of the upper limit for the fit parameters. Because the strongest CT state absorption is found for the blend system based on the bimolecular crystal PBTTT:PCBM to the best of our knowledge[9]. In that case, the peak value of the CT state EQE_{PV} is about 5% of the donor EQE_{PV}. However, the CT state absorption strength of the blends studied in this work is lower than that of the bimolecular crystal. Nevertheless, we estimate an error of $\pm$ 0.025 eV could exist for the value of E_{CT} determined using our method. Details regarding the fitting process can be found in the reference[10].

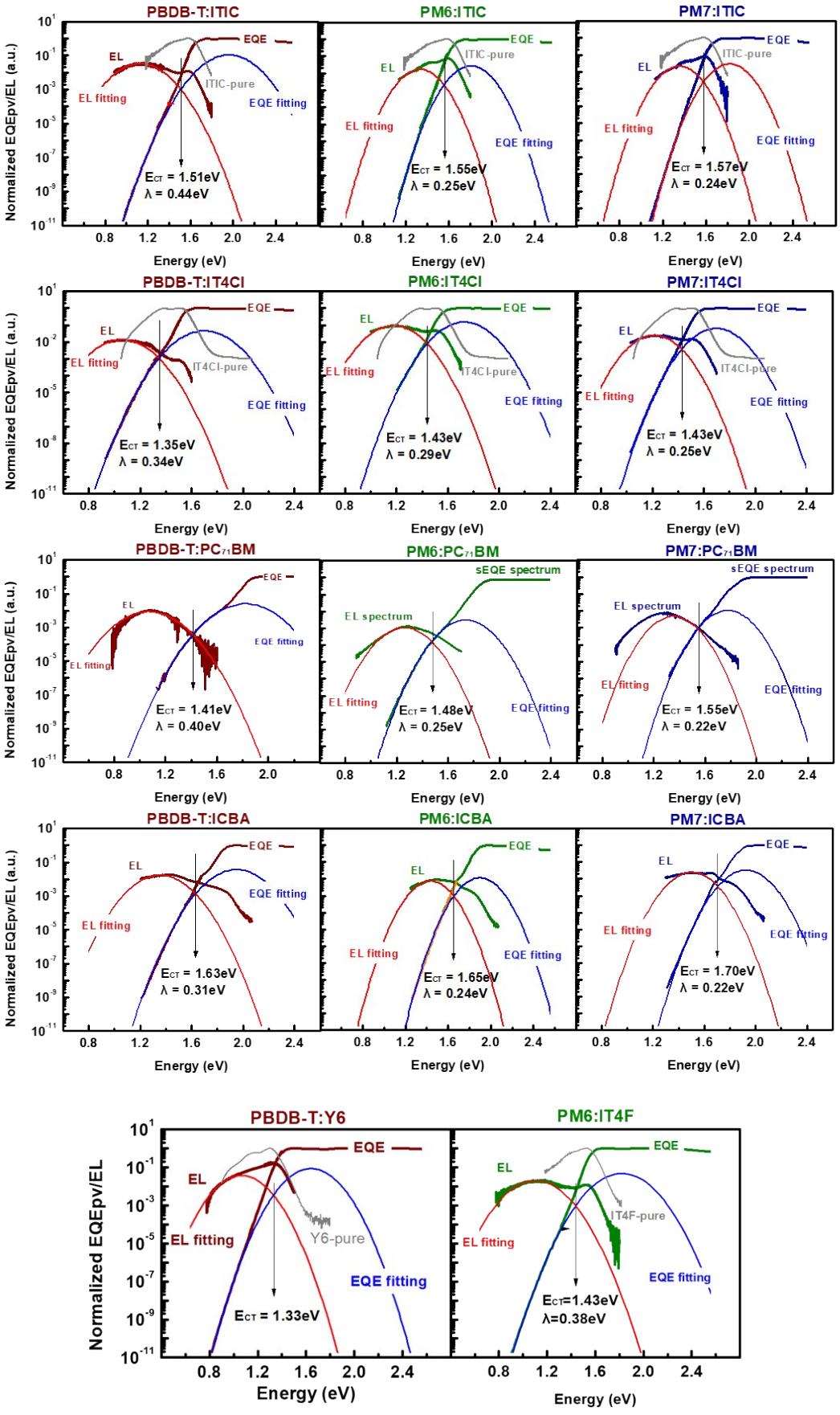

Figure S7. EQE_{PV} and EL spectra of the semitransparent solar cells based on the BHJ systems of non-halogenated and halogenated donors mixed with different acceptors.

Supplementary Note 8. Details regarding the DFT calculations

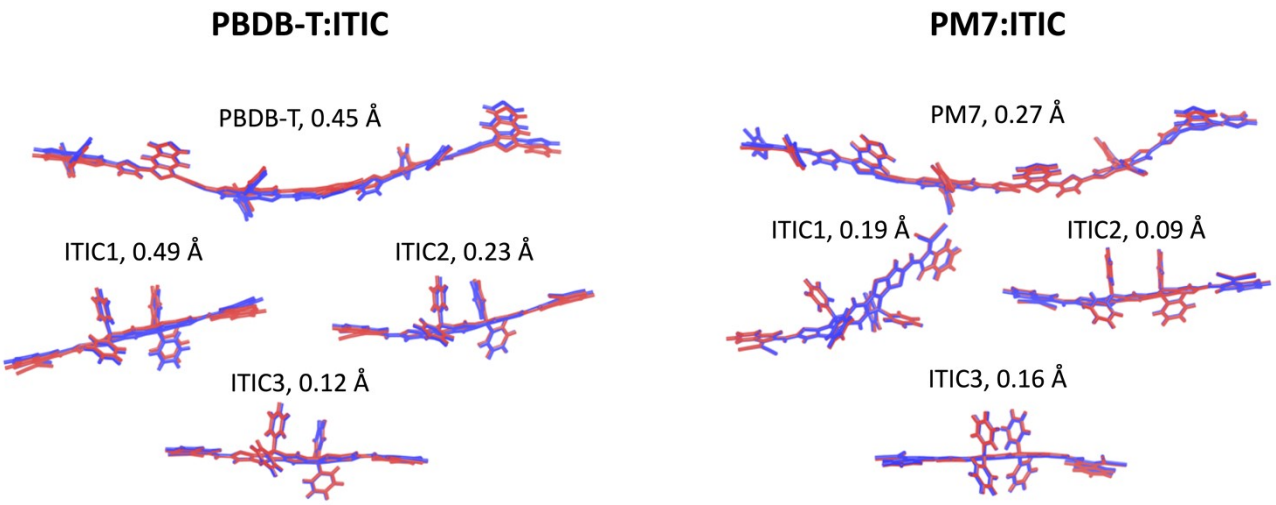

Figure S8. Comparison between the configuration of the donor trimer and the three monomers composing the PBDB-T:ITIC (left) and PM7:ITIC (right) interfaces in the ground (blue) and CT (red) states. We remark that the configurations are drawn after molecule-by-molecule alignment, which minimize the RMSD (also reported in the figure for each species).

Supplementary Note 9. Photoluminescence spectra of the blend films

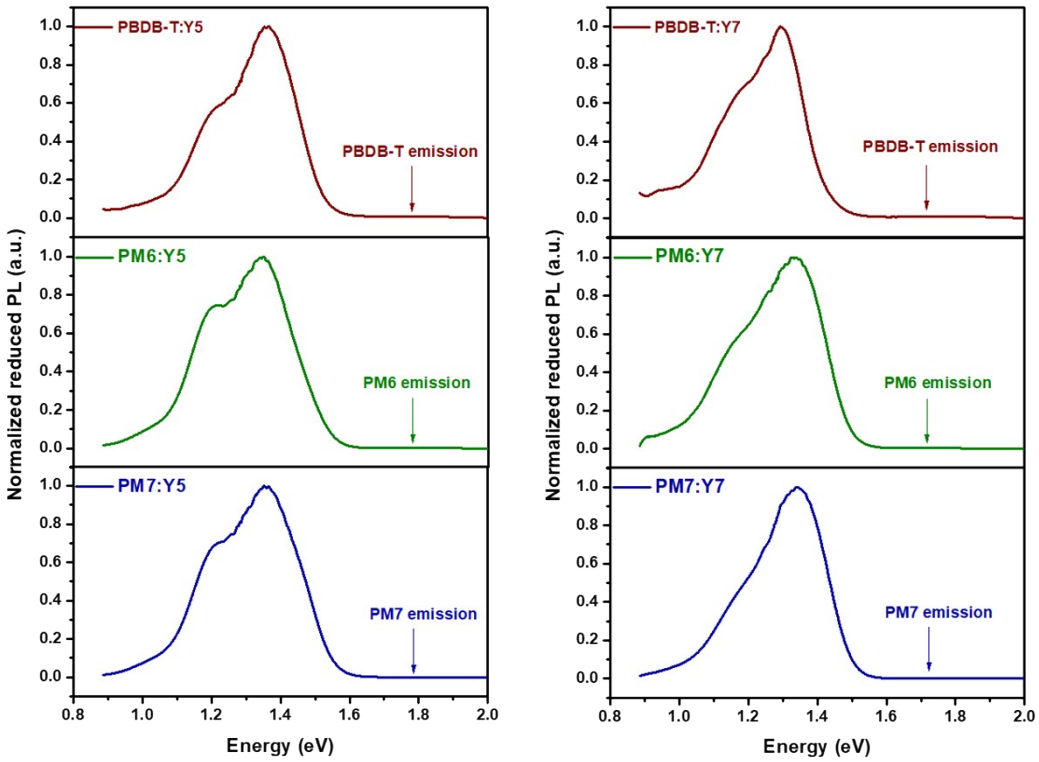

Figure S9. PL spectra for the blend films based on the polymer donors PBDB-T, PM6 and PM7 mixed with Y5 and Y7.

Supplementary Note 10. Details regarding the MD Simulations

In this work, molecular dynamics simulations were carried out by using the materials studio 6.0 software.

Amorphous cell package in the Materials Studio software were utilized to construct initial cubic cells, where the ring spearing and close contacts options were executed. Each cell was composed of 5 polymer chains with 10 repeating units and approximate 40 small molecular acceptor IT4F according to the mass ratio of donor to acceptor (1:1.2). The density of initial cells was set up at very small value of 0.1 g cm^3. The compass force field was used as force field. The side lengths of initial cubic cells were 125.6 Å and 127.8 Å for the PBDB-T:IT4F and the PM7:IT4F systems, respectively; 108.3 Å, 109.8 Å, and 111.30 Å for the PBDTT:IT4F, the PBDTT-1Cl:IT4F, and the PBDTT-2Cl:IT4F systems, respectively; 129.6 Å and 132.2 Å for the PBT1-C:IT4F and the PBT1-C-2Cl:IT4F systems, respectively.

MD simulations were performed with the NPT ensemble from 650 K to 350 K, and finally to 300 K (5 ns) at 1 atmospheric pressure. The cooling process from 650 K to 350 K consists of 4 successive NPT simulations (650 K for 500 ps, 550 K for 500 ps, 450 K for 500 ps, and 350 K for 500 ps). The NPT simulations were carried out using a time step of 1 fs and the Nose-Hoover thermostat/barostat was employed for controlling the temperature and pressure, a cutoff distance for the summation of van der Waals interactions was 12.5 Å. After equilibrium, the side lengths of finally cubic cells were 56.5 Å and 57.3 Å for PBDB-T:IT4F, PM7:IT4F systems; 48.7 Å, 49.0 Å and 49.7 Å for PBDTT:IT4F, PBDTT-1Cl:IT4F and PBDTT-2Cl:IT4F systems; 58.2 Å and 59.6 Å for PBT1-C:IT4F and PBT1-C-2Cl:IT4F systems, separately.

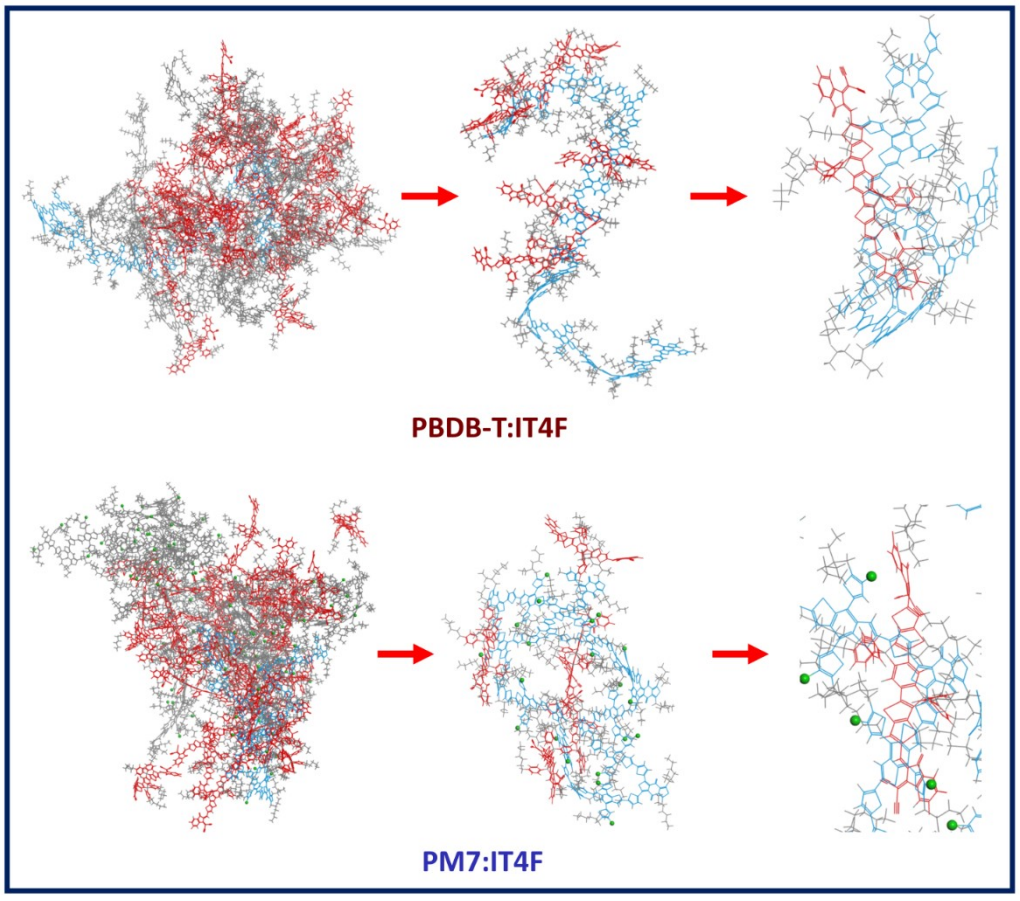

Figure S10. MD simulation results for the DA systems based on PBDB-T:IT4F and PM7:IT4F.

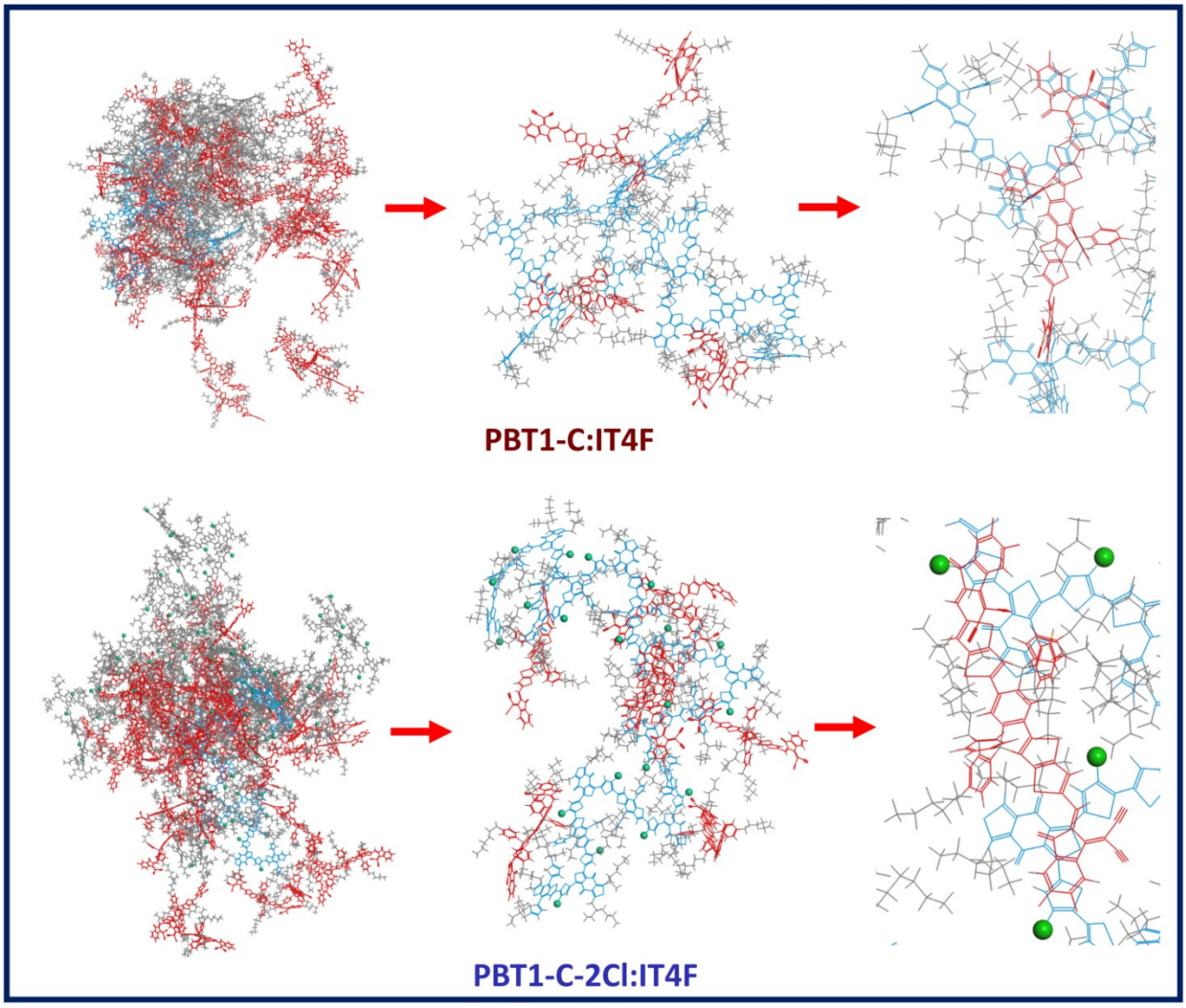

Figure S11. MD simulation results for the DA systems based on PBT1-C:IT4F and PBT1-C-2Cl:IT4F.

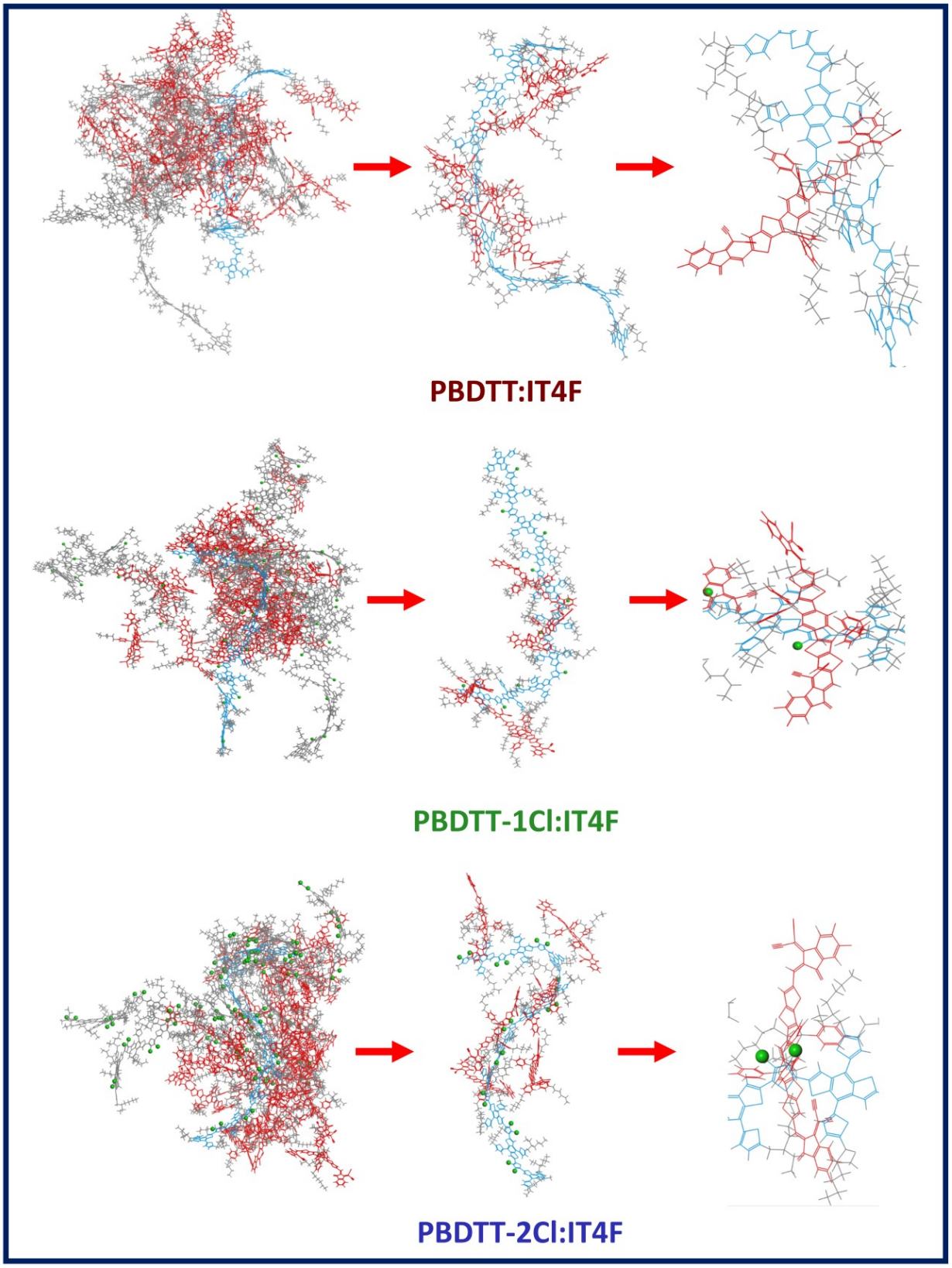

Figure S12. MD simulation results for the DA systems based on PBDTT:IT4F, PBDTT-1Cl:IT4F, and PBDTT-2Cl:IT4F.

References

1. J. Benduhn, K. Tvingstedt, F. Piersimoni, S. Ullbrich, Y. Fan, M. Tropiano, K. A. McGarry, O. Zeika, M. K. Riede, C. J. Douglas, S. Barlow, S. R. Marder, D. Neher, D. Spoltore and K. Vandewal, *Nat. Energy* 2017, **2**, 17053.
2. T. Kirchartz, J. Mattheis and U. Rau, *Phys. Rev. B* 2008, **78**, 235320.
3. C. G. Ribbing, in *Optical Thin Films and Coatings*, Elsevier, 2013, pp. 357–390.
4. U. Rau, *Phys. Rev. B* 2007, **76**, 085303.
5. K. Nakano, Y. Chen, B. Xiao, W. Han, J. Huang, H. Yoshida, E. Zhou and K. Tajima, *Nat. Commun*. 2019, **10**, 2520.
6. M. A. Faist, S. Shoaee, S. Tuladhar, G. F. A. Dibb, S. Foster, W. Gong, T. Kirchartz, D. D. C. Bradley, J. R. Durrant and J. Nelson, *Adv. Energy Mater.* 2013, **3**, 744–752.
7. R. A. Marcus, *J. Phys. Chem.*, 1989, **93**, 3078–3086.
8. K. Vandewal, K. Tvingstedt, A. Gadisa, O. Inganäs and J. V. Manca, *Phys. Rev. B* 2010, **81**, 125204.
9. S. Sweetnam, K. Vandewal, E. Cho, C. Risko, V. Coropceanu, A. Salleo, J.-L. Brédas and M. D. McGehee, *Chem. Mater.* 2016, **28**, 1446–1452.
10. H. Liu, M. Li, H. Wu, J. Wang, Z. Ma and Z. Tang, *J. Mater. Chem. A* 2021, **9**, 1977.